N-XANES spectra if the DNA bases are brominated (*2*). This sensitivity to bromine, and chemical labels with unique spectral signatures, should open up new possibilities in biological microscopy for functional and chemically specific imaging.

XANES spectroscopy provides excellent contrast for high-resolution imaging with chemical specificity. The ability to perform spectroscopy of organic materials 0.01 μm^2 in area and to form high-resolution images that use XANES contrast opens up new areas of study in structural biology and polymer science and in the investigation of other phase-separated materials. Here, we assumed a random, isotropic distribution of the molecules investigated. If explored with a suitable sample or sample rotation stage, the polarization dependence of XANES spectroscopy (*16*) would make it possible for researchers using our technique to determine the direction of specific bonds in oriented systems at high spatial resolution. The possibilities to use chemically specific labels in biology that have unique spectral signatures are particularly intriguing.

REFERENCES AND NOTES

1. R. D. Leapman and S. B. Andrews, *J. Microsc.* **165**, 225 (1992); P. M. Briber and F. J. Khoury, *J. Polym. Sci. Polym. Phys. Ed.* **26**, 621 (1988); L. Reimer, *Transmission Electron Microscopy* (Springer-Verlag, Berlin, 1988).
2. S. M. Kirtley *et al.*, *Biochim. Biophys. Acta*, in press.
3. J. C. Solem and G. C. Baldwin, *Science* **218**, 229 (1982).
4. J. C. Solem and G. F. Chapline, *Opt. Eng.* **23**, 193 (1984).
5. Related EELS spectra of nucleic acids can be found in M. Isaacson [*J. Chem. Phys.* **56**, 1813 (1972)].
6. H. Rarback *et al.*, *J. X-ray Sci. Technol.* **2**, 273 (1990).
7. E. Anderson and D. Kern, in *X-ray Microscopy III*, A. Michette, G. Morrison, C. Buckley, Eds. (Springer-Verlag, Berlin, 1992).
8. C. Jacobsen *et al.*, *Opt. Commun.* **86**, 351 (1991). Although the Rayleigh resolution of our instrument is 55 nm, features smaller than 36 nm have been resolved in test patterns.
9. This corresponds to the first minimum of the modified Airy pattern of our microprobe and contains 59% of the beam intensity.
10. S. J. Wu, *J. Polym. Sci. Polym. Phys. Ed.* **21**, 699 (1983).
11. S. Wu, *Polym. Eng. Sci.* **27**, 335 (1987); S. Cimmino *et al.*, *ibid.* **24**, 48 (1984).
12. S. Wu, *Polymer* **26**, 1855 (1987); R. J. M. Borggreve, R. J. Gaymans, J. Schuijer, J. F. Ingen Housz, *ibid.* **28**, 1489 (1987).
13. J. Cazaux, *Appl. Surf. Sci.* **20**, 457 (1985).
14. P. E. Laibinis, R. L. Graham, H. A. Biebuyck, G. M. Whitesides, *Science* **254**, 981 (1991).
15. S. Williams *et al.*, *J. Microsc.*, in press.
16. J. Stöhr, *NEXAFS Spectroscopy and the Structure of Adsorbed Molecules*, vol. 25 of Springer Series in Surface Science (Springer-Verlag, Berlin, 1992).
17. We used a fourth-order Butterworth filter with a cut-off at 40 cycles for the spectrum with 512 data points.
18. K. Hirayama, A. Satoko, M. Furuya, K. Fukuhara, *Biochem. Biophys. Res. Commun.* **173**, 639 (1990).

19. We are grateful to the many people who have contributed to this work. We particularly thank P. Stevens, who brought the possibilities of C-XANES spectroscopy to our attention. E. Anderson, D. Attwood, and D. Kern provided the zone plate, M. Rivers has been responsible for the data acquisition programs, C. Jacobsen helped implement the XANES acquisition mode, and C. Buckley, C. Jacobsen, S. Lindaas, H. Rarback, and S. Rock made important contributions to STXM development. The polymer samples were prepared by E. Berluche, S. Behal, J. Chludzinski, and S. McCarthy. Supported in part by NSF grant DIR 9005893. This work was performed at the National Synchrotron Light Source, which is supported by the Department of Energy, Office of Basic Energy Sciences.

29 May 1992; accepted 16 September 1992

The Age of Paraná Flood Volcanism, Rifting of Gondwanaland, and the Jurassic-Cretaceous Boundary

Paul R. Renne, Marcia Ernesto, Igor G. Pacca, Robert S. Coe, Jonathon M. Glen, Michel Prévot, Mireille Perrin

The Paraná-Etendeka flood volcanic event produced ~1.5 × 10^6 cubic kilometers of volcanic rocks, ranging from basalts to rhyolites, before the separation of South America and Africa during the Cretaceous period. New $^{40}Ar/^{39}Ar$ data combined with earlier paleomagnetic results indicate that Paraná flood volcanism in southern Brazil began at 133 ± 1 million years ago and lasted less than 1 million years. The implied mean eruption rate on the order of 1.5 cubic kilometers per year is consistent with a mantle plume origin for the event and is comparable to eruption rates determined for other well-documented continental flood volcanic events. Paraná flood volcanism occurred before the initiation of sea floor spreading in the South Atlantic and was probably precipitated by uplift and weakening of the lithosphere by the Tristan da Cunha plume. The Paraná event postdates most current estimates for the age of the faunal mass extinction associated with the Jurassic-Cretaceous boundary.

Continental flood volcanism produces prodigious extrusions of chiefly basalt composition that in several cases exceed a volume of 1 × 10^6 km^3 (*1–3*). At least eight episodes of continental flood volcanism have occurred over the last 250 million years (My), and considerable attention has been devoted to understanding their genesis and relation to a variety of other terrestrial phenomena including hot spots, crustal rifting, and faunal mass extinctions. Detailed dating of several flood volcanic provinces (for example, the Deccan Traps, Siberian Traps, and Columbia River Basalts) has shown that one of the most distinctive features of flood volcanism is a very brief duration of principal activity that lasts 1 or 2 My at most, so that mean eruption rates are on the order of 10^6 km^3/My (*1–3*).

In this paper, we report new $^{40}Ar/^{39}Ar$ geochronologic data on the age and duration of volcanism in the Paraná province, one of the largest known continental flood volcanic provinces. These new data allow evaluation of the temporal relation between Paraná volcanism and the opening of the southern Atlantic Ocean and the Jurassic-Cretaceous mass extinctions.

Connections between flood volcanism, mantle plumes, hot-spot activity, and continental rifting were postulated over 20 years ago (*4*), and several contrasting genetic models for continental flood volcanic events have since emerged. Most models postulate that mantle plumes are responsible (*1–4*) but differ in whether decompression melting of the asthenosphere upon rifting above a preexisting mantle plume generates flood volcanism or, conversely, whether the rise of a mantle plume causes flood volcanism and initiates lithospheric extension (*1–3*). The imprecision in dating of some flood basalt events and associated rifting episodes has precluded confident deduction of their temporal sequence and hence their genetic relations.

A genetic link between flood volcanism and major faunal mass extinctions has been debated vigorously for nearly a decade (*5*), particularly with respect to the Deccan Traps of India and the Cretaceous-Tertiary (K-T) mass extinctions (*5, 6*). Recent dating of the Siberian Traps (*7, 8*) showed that this largest known continental flood volcanic province coincided within uncertainties with the most profound mass extinction event known at the Permian-Triassic boundary ~249 Ma (million years ago). The assessment of further coincidence of

P. R. Renne, Institute of Human Origins Geochronology Center, 2453 Ridge Road, Berkeley, CA 94709.
M. Ernesto and I. G. Pacca, Instituto Astrônomico e Geofísico, Universidade de São Paulo, 05508 São Paulo, Brazil.
R. S. Coe and J. M. Glen, Department of Earth Sciences, University of California, Santa Cruz, CA 95064.
M. Prévot and M. Perrin, Centre Geologique et Geophysique, 34060 Montpelier Cedex, France.

mass extinctions with flood volcanic events has been hindered by a lack of precise geochronologic data for both phenomena.

The Paraná flood volcanic rocks (Serra Geral Formation) currently cover ~1.6 × 10^6 km^2 in the Paraná Basin (Fig. 1) of Brazil, Argentina, Uruguay, and Paraguay (9). On the basis of the distribution of dikes and sills in the basin, the original extent of the volcanics was probably close to 2.0 × 10^6 km^2; the total volume was ~1.3 × 10^6 km^3. An additional 2.5 × 10^5 km^3 of contemporaneous flood volcanic rocks are exposed in Namibia, where they are termed the Etendeka Volcanics (10); these were separated from the Paraná volcanic rocks upon the rifting apart of Gondwanaland in the Cretaceous. The minimum combined original volume of volcanic rocks in the Paraná-Etendeka province is ~1.5 × 10^6 km^3, comparable to that of the Deccan Traps (2). The Paraná and Etendeka provinces are linked to the currently active Tristan da Cunha hot spot via the Rio Grande Rise and Walvis Ridge, respectively. Although their geometries seem to be consistent with hot-spot tracks, such an origin for these lineaments remains to be established.

The Paraná province comprises chiefly tholeiitic basalt and andesite but includes subordinant rhyolites and rhyodacites that are more abundant in the younger parts of the section (9). More than 1500 m of volcanic rocks fill the center of the Paraná Basin (9). Exposed sections generally lack overlying strata, so the original thickness of the volcanic sequence is unconstrained as a result of the unknown amount of material subsequently eroded.

The age and duration of Paraná volcanism have been poorly known. The immediately underlying strata, chiefly eolian sandstones of the Botucatu Formation, are sparsely fossiliferous and have been interpreted only as Triassic or Jurassic, whereas locally overlying terrestrial strata of the Bauru Group are of Late Cretaceous age (11, 12).

More than 200 K-Ar analyses (11), chiefly of whole-rock samples, yield apparent ages concentrated in the range 110 to 150 Ma, with a strongly defined mode at ~127 Ma (Fig. 2). However, many of the K-Ar dates violate stratigraphic constraints on relative ages (13), and the distribution of dates is suspect; both alteration and inherited argon could be responsible for the broad range of apparent ages. In a recent $^{40}Ar/^{39}Ar$ study, regression of isotope correlation trends yielded dates of 133 ± 2 and 132 ± 1 Ma for stratigraphically lower basalts (14). In another recent study (15), $^{40}Ar/^{39}Ar$ data were interpreted to indicate (i) the inception of volcanism at >135 Ma and (ii) the cessation of volcanism at ~130 Ma. Limited Rb-Sr isotopic data from plagioclase, whole-rock, and matrix samples from each of two Paraná rhyodacites yielded an isochron date of 135.5 ± 3.2 Ma (11).

Paleomagnetic data from 20 stratigraphic sections through the Paraná volcanic rocks (Fig. 1) indicate that volcanism spanned four or fewer geomagnetic polarity reversals in any given section (16). In several cases, an apparent reversal is represented by only one rock unit having anomalous polarity (for example, the uppermost reversed polarity rock unit from section TA in Fig. 1), and it is possible that these represent younger sills. Because the geomagnetic field reversed polarity frequently between 140 and 120 Ma (about every 400,000 years on average) (17), it has been postulated that the sequence of volcanic rocks, more than 1000 m thick in several cases, accumulated in less than 1 My in any one section (16). Paleomagnetic data thus undermine the credibility of the broad spectrum of radioisotopic dates but do not clarify the age of volcanism.

We selected samples for $^{40}Ar/^{39}Ar$ dating on the basis of stringent petrographic

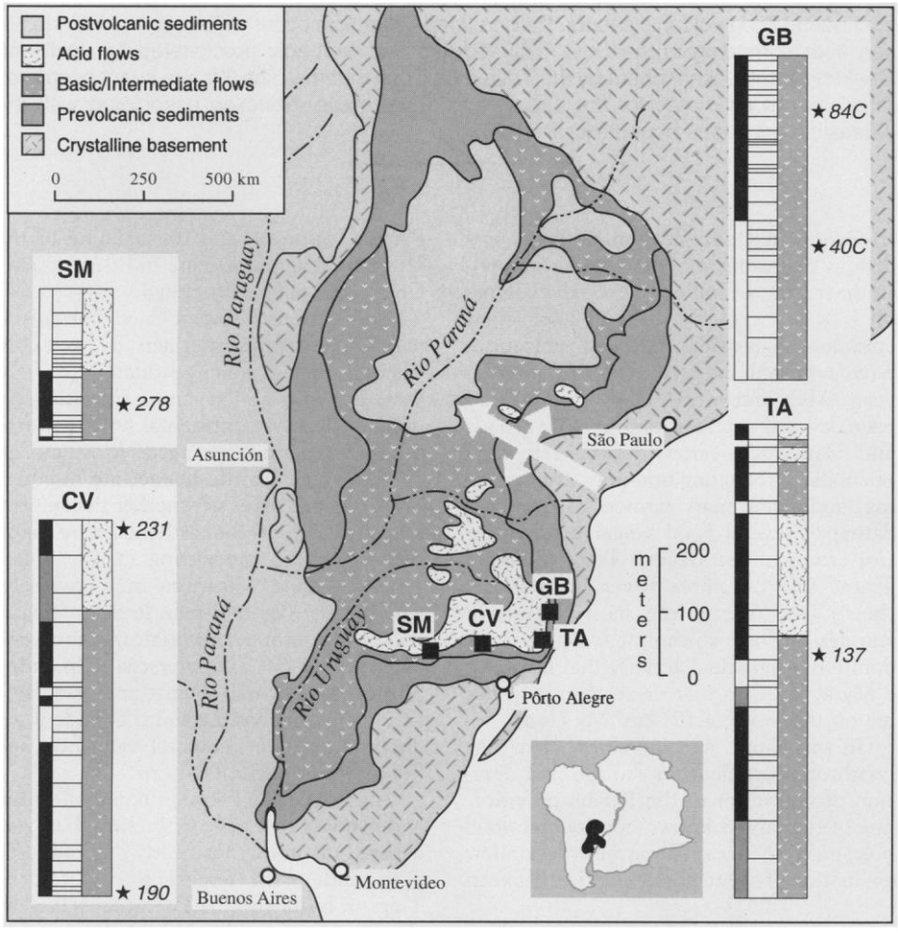

Fig. 1. Geologic map of the Paraná Basin showing the distribution of flood volcanics. Inset shows predrift location of Paraná-Etendeka flood volcanic province. Squares with designations SM, CV, TA, and GB denote locations of stratigraphic sections. Stratigraphic sections show magnetostratigraphy (left column), flow boundaries (middle column), and lithology (right column). In magnetostratigraphic columns, black indicates normal polarity, gray shows transitional directions, and white indicates reversed polarity. Gap near the top of the TA section reflects absence of data. Numbered stars show locations of samples used in this study; the numbers are keyed to Table 1, Fig. 3, and the text. White arrows southwest of São Paulo indicate the location of the Ponta Grossa Arch.

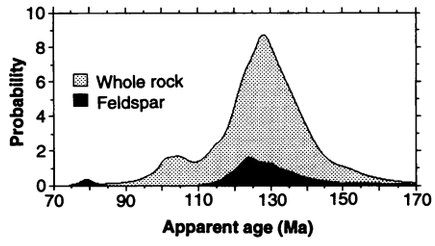

Fig. 2. Probability distribution (ideogram) of 206 K-Ar dates (11) obtained for Paraná flood volcanic rocks. The distribution was obtained by the summation of normal distributions that represent individual dates and analytical uncertainties.

criteria, including a preference for coarse, fresh plagioclase. Whole-rock samples were chosen for their holocrystalline textures, the coarsest possible groundmass grain size, and the absence of alteration products (*18*). Samples were collected as 2.5-cm-diameter cores with a hand-held, gasoline-powered drill from measured sections (Fig. 1).

Sample preparation, facilities, analytical procedures, reduction of Ar isotopic data, and plateau definition criteria were identical to those used in (*7*). Neutron irradiation was for approximately 28 hours. Fish Canyon sanidine (27.84 Ma) was used as a fast neutron fluence monitor, and analysis of ten individual grains yielded a value of $J = 0.006477 \pm 0.000020$, where J is a measure of the fast neutron fluence during irradiation. Optical-grade CaF was irradiated along with the unknown samples in order to monitor the $(^{36}Ar/^{37}Ar)_{Ca}$ and $(^{39}Ar/^{37}Ar)_{Ca}$ nucleogenic production ratios (*19*) to facilitate accurate corrections for nonradiogenic Ar.

Apparent age spectra (Fig. 3 and Table 1) (produced by incremental laser heating) for plagioclase samples produced well-defined plateaus comprising 13 or more steps and spanning more than 85% of the total ^{39}Ar released. Two of the plagioclase (P) samples (SM-278P and CV-231P) displayed minor low-temperature discordance suggestive of partial Ar loss through minor reheating or alteration. The whole-rock (WR) samples were less straightforward, but two of these three yielded acceptable plateaus over more than 60% of the total ^{39}Ar released. The samples that yielded plateaus (CV-190WR and GB-40CWR) both exhibited discordance patterns suggestive of ^{39}Ar recoil. Sample CV-190WR showed the effects of ^{39}Ar recoil loss at low ^{39}Ar release then yielded a plateau as the ^{39}Ar-depleted domains were exhausted. Sample GB-40CWR showed ^{39}Ar recoil loss effects yielding to a nine-step plateau, followed by diminishing apparent ages that probably reflect release of ^{39}Ar recoil-implanted into a refractory, Ca-rich phase such as clinopyroxene (indicated by elevated $^{39}Ar/^{37}Ar$ values for the highest temperature steps). Sample GB-84CWR yielded a discordant spectrum with no plateau and a climbing pattern suggestive of Ar loss or alteration. Petrographic observations (*18*) favor the latter explanation (alteration) for discordance.

Plateau dates from the five samples are mutually indistinguishable in the range 132.9 ± 0.6 Ma to 131.4 ± 1.6 Ma (2σ intralaboratory errors). The youngest and most discrepant, plagioclase from TA-137, was rerun in 18 heating steps that yielded a plateau date of 132.7 ± 1.2 Ma, indistinguishable from the first plateau date but more consistent with the other results. A combined plateau date of 132.5 ± 0.3 Ma was calculated for this sample with the use of all 33 plateau steps from both runs.

The data reveal no evidence of younger dates at the higher stratigraphic levels. Within the CV section, a stratigraphic sequence of volcanic rocks more than 500 m thick is bracketed by lavas dated at 132.6 ± 0.3 Ma (CV-190WR) and 132.8 ± 1.1 Ma (CV-231P). The statistically insignificant time (≤1.1 My 2σ) represented between these two flows encompasses at least two, and possibly four, geomagnetic polarity reversals (Fig. 1). The internal concordance of dates from the CV section and of these with dates from the GB and SM sections, in view of the magnetostratigraphic data, implies that volcanism was essentially synchronous and spanned at most 1 My in the southern Paraná province.

All but 3 of the 20 magnetostratigraphic sections from around the basin begin with a normal polarity interval, and because no systematic spatial trend in initial polarity is discernible, it is possible that volcanism began during the same subchron in >80% of the Paraná Basin. According to recent time scales (*17*), this would correspond to some time between magnetic anomalies M8 and M11; more refined correlation with the magnetostratigraphic time scale is precluded by uncertainties in the numerical calibration of the biostratigraphic time scale and the absence of biostratigraphic calibration for the flood volcanic sequence.

A northward migration of volcanic activity with time has been inferred in other studies (*16, 20*). If volcanism did indeed progress from south to north, then the $^{40}Ar/^{39}Ar$ and paleomagnetic data suggest that this occurred on a time scale of less than 1 My. Furthermore, it is unlikely that volumetrically significant Paraná volcanism occurred earlier than ~133 Ma. The Paraná

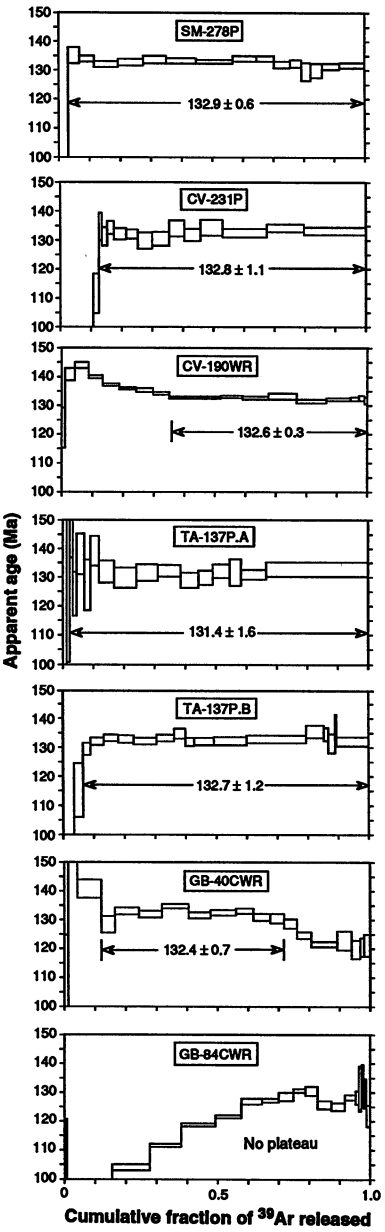

Fig. 3. Apparent age spectra for samples shown in Fig. 1. WR, whole-rock samples; P, plagioclase samples. TA-137P.A and TA-137P.B are replicate analyses of the same sample. Uncertainties, represented by vertical width of bars, are ±1σ and do not include contribution from uncertainty in the neutron fluence parameter J. Plateau dates (indicated in millions years ago) are calculated as described (*19*) with errors at the 2σ level that include analytical uncertainty in J.

Table 1. Summary of $^{40}Ar/^{39}Ar$ plateau data. The Ca/K ratio is equal to 1.96 times the $^{39}Ar_{Ca}/^{37}Ar_K$ ratio and shows the integrated value corresponding to the plateau followed by that for the entire spectrum. The plateau shows the number of steps defining the plateau as a fraction of total steps analyzed; the percentage of total $^{39}Ar_K$ released comprising the plateau is in parentheses. The date is the plateau date, calculated as the inverse variance weighted mean of the plateau step dates.

Sample	Material	Ca/K	Plateau	Date (Ma) ± 2σ
SM-278P	Plagioclase	13.6/13.4	15/16 (97.1)	132.9 ± 0.6
CV-190WR	Whole-rock	1.8/1.4	11/19 (65.0)	132.6 ± 0.3
CV-231P	Plagioclase	30.3/28.3	13/18 (87.6)	132.8 ± 1.1
TA-137P.A	Plagioclase	44.9/44.9	17/17 (100)	131.4 ± 1.6
TA-137P.B	Plagioclase	44.7/44.2	16/18 (93.6)	132.7 ± 1.2
TA-137P.C*	Plagioclase	44.8/44.5	33/35	132.5 ± 0.3
GB-40CWR	Whole-rock	3.6/7.2	9/19 (64.1)	132.4 ± 0.7

*Results for TA-137P.C are combined from replicate analyses of TA-137P.A and TA-137P.B.

province thus fits the emerging general pattern of extremely rapid eruption of flood volcanics. Our best estimate for the inception age of Paraná volcanism is provided by the plateau date for sample CV-190WR: allowing for a possible 1% uncertainty in the age of the neutron fluence monitor (*7*) yields an interlaboratory plateau date for this sample of 132.6 ± 1.3 Ma.

According to one model, derived from the interpretations of marine geophysical data (*21*), Africa and South America separated by progressively unzipping northward from the Falkland Plateau. In this model, the magnetic anomaly closest to the southwesternmost tip of Africa is thought to mark the initiation of sea floor spreading in the South Atlantic and correlates with anomaly M13 of the geomagnetic polarity time scale (GPTS) at 137 to 139 Ma (*17*); 8° to 16° farther north, at latitudes corresponding to the southern Paraná Basin, the oldest sea floor anomaly is M4, formed ~127 Ma (*17*). In this scenario (*3*), therefore, rifting began well south of and presumably unrelated to the Tristan da Cunha plume. It proceeded opportunistically northward toward the hot spot, drawn by the greater extensional deviatoric stress in the uplifted lithosphere above the plume. Weakening and fracturing of the crust unleashed Paraná volcanism at ~133 Ma and led to the formation of the true sea floor there about 5 My later.

The case for this interpretation, however, was weakened by a seismic reflection study (*22*), which showed that the critical magnetic anomalies along the southeastern Atlantic margin of South Africa, previously thought to record the beginning of sea floor spreading, actually occur on thinned continental crust. In this reinterpretation, the oldest sea floor is considerably younger than previously inferred, correlating with anomaly M9 at 129 to 131 Ma (*17*). In the southwestern Atlantic, along the matching margin of Argentina, the situation is clearer: the oldest sea floor anomaly is agreed to be M4 (*21*), which is younger still, having been formed ~127 Ma (*17*). Likewise, farther north along the margin of Uruguay and Brazil, offshore of the southern extent of the Paraná province, a recent synthesis of seismic and well log data (*23*) concludes that the oldest anomaly lying on true sea floor is also M4. Thus, it appears that sea floor spreading commenced almost simultaneously along the southern 2000 km of the South Atlantic rift system 5 My or so after the outpouring of the Paraná flood volcanics.

Off the shore of the northern part of the Paraná province, north of the São Paulo Ridge–Rio Grande Rise, true sea floor spreading did commence significantly later, after anomaly M0 at ~118 Ma (*17*). Here, dramatic stretching of the Brazilian margin associated with the formation of large extensional basins has been documented (*23*). The subsidence histories of these basins are remarkably similar, and many are floored by volcanic rocks tentatively correlated with the Paraná volcanic rocks. Thus, major stretching along this northern segment of the rift occurred after flood volcanism and was coeval with active spreading along the southern segment. The junction of the two rift segments coincides with the Ponta Grossa Arch (*9*) (Fig. 1), a locus of intense dike injection trending northwestward hundreds of kilometers into the Brazilian interior. This feature may be a failed rift (*24*). The dike swarm is not well dated, but its formation between 130 and 118 Ma has been inferred from paleomagnetic data (*16*), and extension in this zone appears capable of accommodating the disparity in rates of separation between the northern and southern rift segments.

Thus, an alternative model that seems more consistent with existing data is one in which the Tristan da Cunha plume played a more central role in continental breakup. By uplifting and weakening the continental lithosphere, the plume precipitated the intense episode of Paraná flood volcanism ~133 Ma. This led within only a few million years to rifting and the initiation of active sea floor spreading almost simultaneously along the entire southern arm of the mid-Atlantic spreading ridge.

Our data also indicate that Paraná volcanism postdates most modern estimates (135 to 145 Ma) (*17*, *25*) for the age of the Jurassic-Cretaceous (J-K) boundary. Some data have been presented in support of an age closer to 130 Ma for the boundary (*26*), but faunal correlations are currently inadequate to assess the synchroneity of the variously defined boundaries at different locations. The preponderance of estimates for the J-K boundary in the range 135 to 145 Ma suggests that temporal correlation is unlikely, but further work on both the definition and the age of the boundary is needed.

REFERENCES AND NOTES

1. K. G. Cox, *J. Petrol.* **21**, 629 (1980); R. S. White *et al.*, *Nature* **330**, 439 (1987); R. S. White and D. P. McKenzie, *J. Geophys. Res.* **94**, 7685 (1989); I. H. Campbell and R. W. Griffiths, *Earth Planet. Sci. Lett.* **99**, 79 (1990); R. A. Duncan and M. A. Richards, *Rev. Geophys.* **29**, 31 (1991); W. J. Morgan, in *The Sea*, C. Emiliani, Ed. (Wiley-Interscience, New York, 1981), vol. 7, pp. 443–475.
2. M. A. Richards, R. A. Duncan, V. E. Courtillot, *Science* **246**, 103 (1989).
3. R. I. Hill, I. H. Campbell, G. F. Davies, R. W. Griffiths, *ibid.* **256**, 186 (1992).
4. W. J. Morgan, *Nature* **230**, 42 (1971); *Am. Assoc. Pet. Geol. Bull.* **56**, 203 (1972).
5. W. J. Morgan, *Eos* **67**, 391 (1986); M. R. Rampino and R. B. Stothers, *Science* **241**, 663 (1988); *Geol. Soc. Am. Spec. Pap.* **247**, 9 (1990).
6. A greenhouse effect caused by volcanogenic CO_2 was postulated as a mechanism for the K-T extinctions [C. O. Officer and C. L. Drake, *Science* **219**, 1383 (1983); D. M. McLean, *Cretaceous Res.* **6**, 235 (1985)]. The K-T mass extinctions have also been attributed to climatic effects of bolide impact [L. W. Alvarez, W. Alvarez, F. Asaro, H. V. Michel, *Science* **208**, 1095 (1980); K. J. Hsü, *Nature* **285**, 201 (1980); W. Alvarez and R. A. Muller, *ibid.* **308**, 718 (1984)].
7. P. R. Renne and A. R. Basu, *Science* **253**, 176 (1991).
8. G. B. Dalrymple, G. K. Czamanske, M. A. Lanphere, V. Stepanov, V. Federenko, *Eos* **72**, 570 (1991).
9. A. J. Melfi, E. M. Piccirillo, A. J. R. Nardy, in *The Mesozoic Flood Volcanism of the Paraná Basin: Petrogenetic and Geophysical Aspects*, E. M. Piccirillo and A. J. Melfi, Eds. (Universidade de São Paulo, Instituto Astronômico e Geofísico, São Paulo, 1988), pp. 1–13.
10. S. C. Milner, *Commun. Geol. Surv. S. W. Afr. Namibia* **2**, 109 (1986).
11. A. C. Rocha-Campos *et al.*, in (*9*), pp. 25–45.
12. P. C. Soares and P. M. B. Landim, *An. Acad. Bras. Cienc.* **48**, 313 (1976).
13. A. J. Melfi, *Geochim. Cosmochim. Acta* **31**, 1079 (1967).
14. C. Hawkesworth *et al.*, in *Magmatism and the Causes of Continental Break-Up*, B. C. Storey, Ed. (Geological Society of London, London, 1991), pp. 13–14.
15. A. J. Baksi, R. V. Fodor, E. Farrar, *Eos* **72**, 300 (1991).
16. M. Ernesto and I. G. Pacca, in (*9*), pp. 229–255; _____, F. Y. Hiodo, A. J. R. Nardy, *Phys. Earth Planet. Inter.* **64**, 153 (1990). Recent K-Ar dating of whole-rock and plagioclase samples of the Ponta Grossa dikes yields dates between 125.1 ± 5.5 and 143.7 ± 6.3 Ma [J. P. P. Pinese, thesis, Universidade de São Paulo (1989)].
17. D. V. Kent and F. M. Gradstein, *Geol. Soc. Am. Bull.* **96**, 1419 (1985); W. B. Harland *et al.*, *A Geologic Time Scale 1989* (Cambridge Univ. Press, Cambridge, 1990). Relevant magnetostratigraphic summaries are given by W. Lowrie and J. G. Ogg [*Earth Planet. Sci. Lett.* **76**, 341 (1986)] and J. E. T. Channell, T. J. Bralower, and P. Grandesso [*ibid.* **85**, 203 (1987)].
18. All the samples analyzed (except CV-231) are holocrystalline basaltic rocks composed mainly of plagioclase, clinopyroxene, olivine (generally pseudomorphed by secondary minerals), and Fe-Ti oxides. The basalts are fine- to medium-grained (average grain size is 100 to 500 μm) and variably porphyritic; samples CV-231 and TA-137 contain phenocrysts of plagioclase up to 2 mm long; these were used for dating. GB-84C, which did not yield a plateau, is the finest-grained sample (grains < 100 μm) and contains secondary celadonite. CV-231 is a porphyritic rhyodacite, with phenocrysts of plagioclase (used for dating) up to 1.5 mm and microphenocrysts of plagioclase, clinopyroxene, and Fe-Ti oxides in a matrix of quartz, alkali feldspars, and altered glass.
19. The nucleogenic production ratios $(^{36}Ar/^{37}Ar)_{Ca}$ and $(^{39}Ar/^{37}Ar)_{Ca}$ that result from nuclear interactions with various Ca isotopes must be accurately and precisely known for age calculations. Isotopic measurements made on CaF irradiated along with the Paraná samples yielded a value of $(^{36}Ar/^{37}Ar)_{Ca} = 2.53 \times 10^{-4} \pm 5.0 \times 10^{-6}$ and $(^{39}Ar/^{37}Ar)_{Ca} = 6.38 \times 10^{-4} \pm 1.0 \times 10^{-5}$. These values are not significantly different from values of $2.56 \times 10^{-4} \pm 4.6 \times 10^{-6}$ and $6.61 \times 10^{-4} \pm 2.5 \times 10^{-5}$ (respectively) determined in independent experiments at the Institute of Human Origins Geochronology Center or from values reported by other laboratories [G. B. Dalrymple *et al.*, *U.S. Geol. Surv. Prof. Pap. 1176* (1981)] using different reactors.
20. D. W. Peate, C. J. Hawkesworth, M. S. M. Montovani, W. Shukowsky, *Geology* **18**, 1223 (1990).
21. P. D. Rabinowitz and J. LaBrecque, *J. Geophys. Res.* **84**, 5973 (1979).

22. J. A. Austin and E. Uchupi, *Am. Assoc. Pet. Geol. Bull.* **66**, 1328 (1982).
23. H. K. Chang, R. O. Kowsmann, A. M. F. Figueiredo, A. A. Bender, *Tectonophysics* **213**, 97 (1992).
24. K. Burke and J. F. Dewey, *J. Geol.* **81**, 406 (1973).
25. M. A. Lanphere and D. L. Jones, in *Contributions to the Geologic Time Scale*, G. Cohee, M. F. Glaessner, H. D. Hedberg, Eds. (American Association of Petroleum Geologists, Tulsa, OK, 1978), pp. 259–268; A. Hallam *et al.*, in *The Chronology of the Geological Record*, N. J. Snelling, Ed. (Blackwell, Palo Alto, CA, 1985), pp. 118–140; T. J. Bralower, K. R. Ludwig, J. D. Obradovich, D. L. Jones, *Earth Planet. Sci. Lett.* **98**, 62 (1990).
26. Y. Bodan, *Phanerozoic Time Scale Bull. Liaison I.U.G.S. Subcomm. Geochronol.* **7**, 31 (1988); G. S. Odin, B. Galbrun, M. Renard, *ibid.* **10**, 39 (1992).
27. This research was supported by the Institute of Human Origins and NSF grants EAR-9209719 to P.R.R. and EAR-8916832 to R.S.C. We are grateful to M. S. D'Agrella for field assistance; R. A. Duncan, D. V. Kent, A. J. Melfi, and A. J. R. Nardy for discussion; G. H. Curtis, R. I. Hill, D. Mertz, E. M. Piccirillo, and M. A. Richards for comments on the manuscript; A. Jaouni and F. Drayer for sample preparation; and D. Beckner for Fig. 1 graphics.

29 June 1992; accepted 9 September 1992

A Prediction of Mars Seismicity from Surface Faulting

Matthew P. Golombek, W. Bruce Banerdt, Kenneth L. Tanaka, David M. Tralli

The shallow seismicity of Mars has been estimated by measurement of the total slip on faults visible on the surface of the planet throughout geologic time. Seismicity was calibrated with estimates based on surface structures on the moon and measured lunar seismicity that includes the entire seismogenic lithosphere. Results indicate that Mars is seismically active today, with a sufficient number of detectable marsquakes to allow seismic investigations of its interior.

The level of tectonic and geologic activity on Mars suggests that it should be seismically more active than the moon but less active than the Earth (*1*). Although the Viking seismometer failed to detect a marsquake, the poor sensitivity of the instrument does not preclude Mars from being a seismically active planet (*2*). In addition, calculations (*1*) indicate that stresses induced by cooling of the martian lithosphere should give rise to seismicity that exceeds the rate of shallow lunar seismicity (28 events in 8 years) thought to be of tectonic origin (*3*).

The seismic scalar moment is defined as $M_o = \mu S A_f$, with uniform rigidity μ and average slip S over fault area A_f. Measurement of the total slip on a fault of known or estimated depth and length allows a determination of the cumulative seismic moment. This value provides an estimate of the total seismic energy released by simple double-couple source mechanisms. The release of the total seismic moment can be distributed according to event size by an assumed relation between moment and frequency of occurrence.

Tectonic features on Mars are found primarily around the Tharsis region, a large elevated volcanic plateau with associated tectonic features that cover the entire western hemisphere of the planet. Tharsis tectonism has occurred mainly during two periods (*4*, *5*), the Late Noachian–Early Hesperian and the Late Hesperian–Early Amazonian. They correspond to time periods of 3.8 to 3.1 billion years ago (Ga) or 4.0 to 3.7 Ga, and 3.1 to 0.7 Ga or 3.7 to 2.5 Ga, respectively, depending on which crater–absolute time scale is used to calibrate martian stratigraphy (*6*). Tectonic features that formed during the first period include (i) a dense radial swarm of narrow grabens, (ii) a sweeping system of concentric wrinkle ridges, (iii) large grabens and rifts of Tempe Terra, and (iv) deep rift valleys of Valles Marineris. Structures that formed during the second period include (i) an enormous set of radial grabens that extend up to thousands of kilometers from the center of the plateau; (ii) large, particularly dense grabens around Alba Patera; (iii) rift zones of Valles Marineris; and (iv) the Thaumasia rift, on the south flank of Tharsis. Tectonism and volcanism continued through the Middle and Late Amazonian (perhaps to the present) at lower levels. Faulting during the Middle Amazonian [0.7 to 0.25 Ga or 2.5 to 0.7 Ga (*6*)] was localized around the center of the plateau and around the large Tharsis Montes volcanoes. Late Amazonian [0.25 or 0.7 Ga to the present (*6*)] faulting surrounded the Tharsis Montes volcanoes and was associated with late stage caldera collapse. Faulting also continued in the rift valleys of Valles Marineris throughout Middle and Late Amazonian time.

The most common tectonic feature on Mars is the simple graben (*7*), which is bounded by two ~60° inward-dipping normal faults (*8*). These faults extend about 2.5 km into the martian interior and have experienced an average of 150 m of slip (*9*). Faulting on narrow grabens has been estimated from a data set (*10*) that includes the locations and lengths of all visible grabens (approximately 7000), about half of which formed during each of the two tectonic periods (*4*, *5*).

Larger grabens and rifts that involve more of the lithosphere are also found on Mars, principally in Valles Marineris, Thaumasia, Tempe Terra, and Alba. Faults bounding the Thaumasia rift (from the Late Hesperian to Early Amazonian periods) and the canyons in Valles Marineris (from both periods) likely extend through the entire brittle lithosphere, estimated to be ~40 km thick (*7*). Slip was determined from the observed topographic relief (4 to 8 km for Valles Marineris, 1.5 km for the Thaumasia rift). Geologic mapping of Valles Marineris (*11*) indicates that trough-bounding faults tens of kilometers long cut Amazonian landslides and floor materials in the canyons and have offset trough walls as much as several hundred meters. On the basis of these relations, the latest fault activity in Valles Marineris during Middle and Late Amazonian time is represented as 20 faults, each 50 km long and having undergone 100 m of slip. Grabens at Alba and Tempe Terra are more narrow and probably involve the upper 5 to 10 km of the lithosphere (*7*). Grabens at Alba formed mostly during the Early Amazonian and have experienced 0.2 to 0.5 km of slip (*12*). Tempe Terra rifts appear to be ~0.5 km deep and were formed in the Late Noachian (*4*). Fault lengths were measured directly from surface maps.

Abundant compressional wrinkle ridges around Tharsis formed during the Early Hesperian. A model in which subsurface thrust faults were assumed to dip about 25° and extend 5 km down dip with ~150 m of slip (*13*) was applied to the lengths of about 2000 ridges around Tharsis (*10*). In addition, the length, average width, and depth of Middle and Late Amazonian grabens were measured to derive fault areas and slips for the two youngest time periods. Caldera collapse also was included in the measurements of Late Amazonian activity because a detailed seismological study (*14*) on Earth shows that collapse occurs by an equivalent shear process and produces fairly large earthquakes. The length, extent [10 km deep (*15*)], and slip [from present relief (*16*)] of circular caldera faults on the tops of Olympus, Ascraeus, Pavonis, and Arsia Mons were included in Late Amazonian

M. P. Golombek, W. B. Banerdt, D. M. Tralli, Jet Propulsion Laboratory, Mail Stop 183-501, California Institute of Technology, Pasadena, CA 91109.
K. L. Tanaka, U.S. Geological Survey, Flagstaff, AZ 86001.